



HAL
open science

CD90 Expression Controls Migration and Predicts Dasatinib Response in Glioblastoma

Tony Avril, Amandine Etcheverry, Raphael Pineau, Joanna Obacz, Gwenaele Jegou, Florence Jouan, Pierre-Jean Le Reste, Masumeh Hatami, Rivka R. Colen, Brett L. Carlson, et al.

► **To cite this version:**

Tony Avril, Amandine Etcheverry, Raphael Pineau, Joanna Obacz, Gwenaele Jegou, et al.. CD90 Expression Controls Migration and Predicts Dasatinib Response in Glioblastoma. *Clinical Cancer Research*, 2017, 23 (23), pp.7360-7374. 10.1158/1078-0432.CCR-17-1549 . hal-01671761

HAL Id: hal-01671761

<https://univ-rennes.hal.science/hal-01671761>

Submitted on 15 Mar 2018

HAL is a multi-disciplinary open access archive for the deposit and dissemination of scientific research documents, whether they are published or not. The documents may come from teaching and research institutions in France or abroad, or from public or private research centers.

L'archive ouverte pluridisciplinaire **HAL**, est destinée au dépôt et à la diffusion de documents scientifiques de niveau recherche, publiés ou non, émanant des établissements d'enseignement et de recherche français ou étrangers, des laboratoires publics ou privés.

CD90 expression controls migration and predicts dasatinib response in glioblastoma.

Tony Avril^{1,2}, Amandine Etcheverry³, Raphaël Pineau¹, Joanna Obacz¹, Gwénaële Jegou^{1,2}, Florence Jouan¹, Pierre-Jean Le Reste^{1,4}, Masumeh Hatami⁵, Rivka R. Colen^{5,6}, Brett L. Carlson⁷, Paul A. Decker⁷, Jann N. Sarkaria⁷, Elodie Vauléon^{1,2,3}, Dan Cristian Chiforeanu⁸, Anne Clavreul⁹, Jean Mosser³, Eric Chevet^{1,2,*}, Véronique Quillien^{1,2,3,*}.

¹Proteostasis & Cancer Team, INSERM U1242 « Chemistry, Oncogenesis Stress Signaling », Université de Rennes 1, Rennes, France ; ²Centre Eugène Marquis, Rennes, France ; ³Integrated Functional Genomics and Biomarkers Team, UMR6290 CNRS, Université de Rennes 1, Rennes, France ; ⁴Département de Neuro-Chirurgie, CHU Pontchaillou, Rennes, France ; ⁵Department of Cancer Systems Imaging, University of Texas, MD Anderson Cancer Center, Houston, United-States of America ; ⁶Department of Diagnostic Radiology, University of Texas, MD Anderson Cancer Center, Houston, United-States of America; ⁷Department of Radiation Oncology, Mayo Clinic, Rochester, United States of America ; ⁸Département d'Anatomo-pathologie, CHU Pontchaillou, Rennes, France ; ⁹Département de Neuro-Chirurgie, CHU Angers, France.

* equally contributed to this work.

Running title: CD90 controls GBM migration.

Correspondence to: Tony Avril, Centre Eugène Marquis, Rue de la bataille Flandres Dunkerque, CS44229, 35042 Rennes cedex, FRANCE. Email: t.avril@rennes.unicancer.fr.

Grant support: This work was supported by grants from «la Ligue Contre le Cancer» Comité d’Ille-et-Villaine, d’Indre-et-Loire et du Morbihan to TA ; Région Bretagne «AAP CRITT santé 2013» and «Aidez la recherche!» from the Centre Eugène Marquis to VQ and la « Ligue Contre le Cancer» Comité des Landes (LARGE project), l’Institut National du Cancer (INCa_5869, INCa_7981, PLBIO: 2015-111) and EU H2020 MSCA ITN-675448 (TRAINERS) to EC.

Abbreviations: CI for confidence interval; FBS for foetal bovine serum; GBM for glioblastoma; GASC for glioblastoma associated stromal cell; GSC for glioblastoma stem cell; GPI for glycoposphatidylinositol; RADH for adherent cell line; RNS for neurosphere cell line; VASARI for Visually Accessible Rembrandt Images.

Authors’ contributions: TA conceptualized the project, designed and performed the experiments, analyzed data and wrote the manuscript; AE analyzed the transcriptome data; RP and FJ performed *in vivo* experiments; JO and GJ performed the cell cultured based experiments and Western-blot with primary cells; PJLR, EV and DCC provided clinical samples and data; MH and RRC provided MRI data; BC, PAD and JNS provided TMA data; AC designed the *in vivo* data; JM designed experiments and analyzed data; EC conceptualized, designed and analyzed the signaling data and wrote the manuscript; VQ designed experiments, analyzed data and wrote the manuscript.

Competing interests: The authors disclose no potential conflicts of interest.

STATEMENT OF TRANSLATIONAL RELEVANCE

CD90/Thy-1 is considered as a surrogate marker for stem cells including glioblastoma (GBM) stem cells (GSCs). In the present study, we demonstrated that CD90 is not only expressed on GSCs but also on more differentiated GBM cells. In GBM patients, CD90 expression was associated with an adhesion/migration gene signature and invasive tumor features as observed by MRI. In GBM cells, modulation of CD90 expression dramatically impacted on adhesion/migration properties. Moreover, orthotopic xenografts revealed that CD90 overexpression induced invasive phenotypes *in vivo*. Furthermore, we showed that CD90 signals through SRC and FAK in both cellular models and GBM specimens. Remarkably, the SRC inhibitor dasatinib blunted CD90-dependent invasion *in vitro* and *in vivo* thereby suggesting its potential use for CD90^{high} tumors. Hence, we demonstrate that CD90 plays a key role in GBM invasiveness through SRC-dependent mechanisms and could be used as a predictive factor for dasatinib response in CD90^{high} GBM patients.

ABSTRACT

Purpose: CD90 (Thy-1) is a glycoposphatidylinositol-anchored glycoprotein considered as a surrogate marker for a variety of stem cells including glioblastoma (GBM) stem cells (GSCs). However, the molecular and cellular functions of CD90 remain unclear.

Experimental design: The function of CD90 in GBM was addressed using cellular models from immortalized and primary GBM lines, *in vivo* orthotopic mouse models, GBM specimens' transcriptome associated with MRI features from GBM patients. CD90 expression was silenced in U251 and GBM primary cells; and complemented in CD90 negative U87 cells.

Results: We showed that CD90 is not only expressed on GSCs but also on more differentiated GBM cancer cells. In GBM patients, CD90 expression was associated with an adhesion/migration gene signature and with invasive tumor features. Modulation of CD90 expression in GBM cells dramatically impacted on their adhesion and migration properties. Moreover, orthotopic xenografts revealed that CD90 expression induced invasive phenotypes *in vivo*. Indeed, CD90 expression led to enhanced SRC and FAK signaling in our GBM cellular models and GBM patients' specimens. Pharmacologic inhibition of these signaling nodes blunted adhesion and migration in CD90 positive cells. Remarkably, dasatinib blunted CD90 dependent GBM cell invasion *in vivo* and killed CD90^{high} primary GSC lines.

Conclusion: Our data demonstrate that CD90 is an actor of GBM invasiveness through SRC dependent mechanisms and could be used as a predictive factor for dasatinib response in CD90^{high} GBM patients.

Key words: CD90/Thy-1 ; glioblastoma ; cell migration ; dasatinib

INTRODUCTION

Glioblastoma (GBM) is one of the deadliest human cancers with an incidence of about 3.5/100,000 per year worldwide (1). Despite the aggressive standard of care currently used including surgery, chemo- and radiotherapy, the prognosis remains very poor with ~15 months overall survival (2). The inevitable recurrence of GBM is associated with: (i) resistance to radio- and chemo-therapy; (ii) diffuse features due to the invasiveness properties of tumor cells throughout the surrounding brain parenchyma and (iii) tumor intra- and inter-heterogeneity (1, 3).

CD90 (Thy-1) is a marker for mesenchymal stromal/stem cells (4) that has been earlier described in glioma/GBM specimens (5) and immortalized glioma/GBM cell lines (6-10). In the past years, CD90 has been described as a human GBM stem cell (GSC) marker (11-15). CD90 is also expressed in GBM-associated stromal cells (GASCs) (16) and mesenchymal stem cell-like pericytes (17), thereby reflecting GBM cellular heterogeneity. CD90 is a N-glycosylated, glycoposphatidylinositol (GPI)-anchored cell surface protein, originally described in murine thymocytes (18). CD90 is also expressed in many other cell types including endothelial cells, fibroblasts and neurons (4, 19-21). CD90 has been involved in neurite outgrowth inhibition, T-cell activation and apoptosis, leukocytes and melanoma cell adhesion and migration, tumor suppression in ovarian cancers; and fibroblast proliferation and migration in wound healing and fibrosis (19, 21). Although the exact mechanisms of action of CD90 remain ill-defined, a role in cell-cell/matrix interactions has been proposed (19, 21).

We show that CD90 expression is not only restricted to GBM stem-like cells but is also observed in more differentiated GBM cells (primary adherent lines) and in freshly dissociated GBM specimens. In GBM patients, CD90 is associated with a cell adhesion/migration gene signature and with multifocal/multicentric MRI features. Using *in vitro* and *in vivo* approaches, we demonstrate the critical role of CD90 in GBM migration/invasion. We show that CD90

signaling through SRC, FAK and RhoA promotes cell migration and importantly, that high CD90 expression impacts on the cell response to the SRC inhibitor dasatinib. We propose a model in which CD90 expression represents a novel stratification tool for selecting patients to be treated with dasatinib. Moreover, in this model, dasatinib could not only impair the adhesion/migration of CD90^{high} differentiated tumor cells but also the proliferation of CD90^{high} GSCs, thereby increasing its therapeutic potential for CD90^{high} patients.

MATERIALS AND METHODS

Reagents and antibodies - All reagents not specified below were purchased from Sigma-Aldrich (St Quentin Fallavier, France). Antibodies against human CD31, CD45, CD90, CD200, FAK, phosphoFAK and VCP were obtained from BD Biosciences (Le Pont de Claix, France); anti-CD90 antibody used for immunohistochemistry from Novus Biologicals (Bio-Techne, Lille, France); anti-CD133 antibody from Miltenyi Biotec (Paris, France); and anti-IL13R α 2 antibody from Biolegend (Ozyme, St Quentin Yvelines, France); anti-phosphotyrosine antibody from Thermofisher (Brebieres, France); anti-SRC and anti-phosphoSRC antibodies from Cell Signaling Technology (Saint Quentin Yvelines, France); and anti-vimentin antibody from Dako (Les Ulis, France).

Tumor specimens and cell culture - GBM samples were obtained after informed and written consent from patients admitted to the neurosurgery department at Rennes University Hospital for surgical resection in accordance with the local ethic committee and the French regulations. Tumors used in this study were histologically diagnosed as grade IV astrocytoma according to the WHO criteria. For transcriptome analysis, we retrospectively recruited a local cohort of 77 GBM patients (males: n=54; females: n=23; median age = 60 years - from 36 to 75 years; recruited between 2004 and 2013) treated with radiotherapy and concurrent/adjuvant temozolomide in accordance with the standard of care (Table S1). Tumor samples were snap-frozen immediately after resection. All samples presented at least 70% of tumor cells. The extent of surgery was evaluated with an enhanced magnetic resonance imaging (MRI) performed within 24 hours after the resection. Adherent (RADH) and neurospheres (RNS) (enriched in stem cells) GBM primary cell lines were obtained from GBM samples as described in (22, 23). Briefly, fresh tumor tissues were mechanically dissociated using gentleMACS dissociator following the manufacturer's instructions (Miltenyi Biotec). Cells were directly cultured and frozen before

further use such as flow cytometry analysis. RADH cells were grown in Dulbecco's Modification of Eagle's Medium (DMEM, Lonza, Verviers, Belgium) supplemented with 10% foetal bovine serum (FBS) (Lonza). RNS cells were grown in DMEM/Ham's:F12 (Lonza) supplemented with B27 and N2 additives (Invitrogen, Cergy Pontoise, France), EGF (20 ng/ml) and basic FGF (20 ng/ml) (Peprotech, Tebu-Bio). All GBM RNS and RADH cells were used between the 5th and 15th passages for the experiments. Human immortalized U251 and U87 GBM cell lines were cultured in DMEM 10% FBS.

Preparation of CD90 knocked-down U251 and CD90 expressing U87 GBM cell lines - U251 cells were transfected with pLKO.1-puro plasmids containing shRNA constructs #24 (5'-ccggcgaaccaacttcaccagcaaaactcgagtttgctggtgaagttggttcgttttg-3') and #25 (5'-ccgggctcagagacaaactggcaactcgagttgaccagttgtctctgagcttttg-3') targeting CD90 mRNA and #CTR (5'-ccggcaacaagatgaagagcaccaaactcgagttggtgctcttcatcttgtgtttt-3') targeting non-mammalian mRNA (Sigma-Aldrich) using the Lipofectamine 2000 reagent (Life Technologies, St Aubin, France) according to the manufacturer's instructions. After one week of culture under the selective antibiotic puromycin used at 10 µg/ml, transfected U251 cells were amplified and then cloned in 96-well plates at 0.1 cell/well. CD90 knocked-down U251 cell lines were expanded and selected for their decreased expression of CD90. U87 cells were transfected with CD90 cDNA (GeneWiz, Sigma-Aldrich) cloned into the pLKO.1-puro plasmid with EcoRI and BamHI enzymes using the Lipofectamine 2000 reagent. CD90 expressing U87 cell lines were obtained as described above with U251 and were selected for their high expression of CD90.

Preparation of CD90 knocked-down RNS GBM primary cell lines - RNS cells were infected with lentiviral particles generated from HEK293T cells using Lenti-X packaging single shot system (Takara, Ozyme) and pLKO.1-puro plasmids containing shRNA constructs #25 targeting CD90

mRNA and #CTR targeting non-mammalian mRNA according to the manufacturer's instructions. After one week of culture under puromycin selection used at 10 µg/ml, RNS cells were amplified and selected for their down-regulation of CD90 expression.

Orthotopic mouse model - Eight-weeks old male Balb/c NOD-SCID mice (Janvier, Saint Berthevin, France) were housed in an animal care unit authorized by the French Ministries of Agriculture and Research (Biosit, Rennes, France - Agreement No. B35-238-40). Parental, transfected U87 cells (50,000 cells/mouse) and RNS cells (50,000 cells/implantation) were orthotopically implanted in immunocompromised mice as described in (24). Mice were daily clinically monitored and sacrificed 28 days after implantation. Mouse brains were collected, fixed in formaldehyde solution 4% and paraffin embedded for histological analysis after H&E staining. Tumor burden was compared in the different groups of mice and analyzed using ImageJ software (25). For dasatinib treatment, mice were fed daily with dasatinib (40 mg/kg, Selleckchem, Euromedex, Souffelweyersheim, France) one week after implantation and for 3 weeks.

Gene expression data analysis - CD90 mRNA expression data were assessed from the publicly available datasets obtained with immortalized cell lines (GDS4296) (26), glioma cell lines (GDS3885) (27), and glioma specimens (GDS1815) (28), (GDS1975) (29), (GDS4465) (30) and (GDS4470) (31); stored in the Gene Expression Omnibus (GEO) repository of the NCBI website platform <http://www.ncbi.nlm.nih.gov/geo/profile/>. Expression levels of CD90 mRNA were expressed as \log_2 (fluorescence intensities) determined in the different microarray datasets. For transcriptome analysis using a local GBM cohort, total RNA was isolated with the NucleoSpin RNAII Kit (Macherey-Nagel, Hoerdt, France). RNA integrity (RNA Integrity Number ≥ 8) was confirmed with an Agilent 2100 bioanalyzer (Agilent Technologies, Les Ulis, France). Gene

expression profiling was carried out with the Agilent whole human genome 8x60K microarray kit (Agilent Technologies). Total RNA was extracted, labelled and hybridized according to the kit manufacturer's recommendations. Raw intensity data were log₂-transformed and normalized (intra-array and inter-array scaling) using *GeneSpring* software (Agilent Technologies). Student *t*-tests with a Welch approximation were used to compare expression values between conditions. Adjusted *p* values were calculated by controlling for the false discovery rate with the Benjamini & Hochberg procedure. Genes were considered significantly differentially expressed if the *p* value was below 0.05 and the absolute fold-change was greater than 2.

Western blotting - Cells were lysed in ice-cold lysis buffer (30 mM Tris-HCl, pH 7.5, 150 mM NaCl, 1.5% CHAPS). Proteins were resolved by SDS-polyacrylamide gel electrophoresis (12%, 10% and 7% polyacrylamide gels for FAK, phosphotyrosine and SRC proteins respectively) and transferred to nitrocellulose membrane for blotting. The membranes were blocked with 3% bovine serum albumin in 0.1% Tween 20 in PBS and incubated with the diluted primary antibodies (1/1000). Antibody binding was detected with the appropriate horseradish peroxidase-conjugated secondary antibodies (1/7000) (anti-rabbit or anti-mouse) (Dako) and visualized with ECL (KPL, Eurobio, Courtaboeuf, France) according to the manufacturer's instructions. Kinase phosphorylation intensities were relative to total corresponding kinase signals using ImageJ.

Immunohistochemistry - Human GBM and mouse brain sections were deparaffinized with EZ prep solution (Ventana Medical Systems, Tucson, United-States of America) at 75°C for 8 minutes. Antigen retrieval was performed using Tris based buffer solution CC1 at 95°C for 48 minutes and endogen peroxidase was blocked. After rinsing, slides were incubated at 37°C for 60 minutes with diluted primary antibodies against antigens (1/300 and 1/50 dilutions for vimentin and CD90, respectively). Signal enhancement was performed using the DABMap kit

(Ventana Medical Systems). Detection kit procedure was optimized on the discovery instrument (Ventana Medical Systems).

Flow cytometry - Cells were washed in PBS 2% FBS and incubated with saturating concentrations of human immunoglobulins and fluorescent-labelled primary antibodies for 30 minutes at 4°C. Cells were then washed with PBS 2% FBS and analyzed by flow cytometry using a FACSCanto II flow cytometer (BD Biosciences). The population of interest was gated according to its FSC/SSC criteria. In most of the experiments, the dead cell population was excluded using 7-amino-actinomycin D (7AAD) staining (BD Biosciences). Data were analyzed with the FACSDiva (BD Biosciences) or the FlowJo software (Tree Star Inc., Ashland, United States) and the results were expressed as specific fluorescence intensity given by the ratio of geometric mean of test / geometric mean of the isotype control. For intracellular staining of phosphoSRC, cells were previously fixed with methanol overnight at -20°C and then permeabilized using the eBioscience fixation/permeabilization kit (Thermofisher). Cells were then incubated with anti-phosphoSRC antibody (Cell Signaling Technology) for 30 minutes at 4°C. After washing with permeabilization solution (eBiosciences), cells were finally stained with secondary anti-rabbit antibody (Millipore, Merck, Molsheim) and directly analyzed by flow cytometry.

Cell viability - RNS cells were cultured in 96-well plates at 25,000 cells/well in the presence of graduale amount of dasatinib (from 0 to 100 µM) (Selleckchem). After 5 days of culture, 20 µl of the WST1 reagent (Roche, Meylan, France) were added in each well. After 4 hours at 37°C, optic densities (OD) were analyzed by spectrophotometry at 450 and 595 nm. Specific OD were given by the difference between the OD observed at 450 nm and the OD observed at 595 nm. The cell viability was calculated by the ratio of the specific OD observed with cells incubated in

the presence of different concentration of dasatinib and the specific OD observed with cells cultured in medium alone.

Cell-matrix adhesion assay - 96-well plates were coated with a filtered solution of 400 µg/ml rat tail collagen I in PBS (Sigma, St Louis, MO, USA). Parental, controls and transfected U251 and U87 cells (25,000 cells) were plated for time points 0, 30 minutes, 1, 2 and 4 hours. Medium and unattached cells were aspirated. Wells were washed with PBS and attached cells were stained with the WST1 reagent as described above. The percentage of cell attachment was calculated by the ratio of the specific OD observed with tested cells and the specific OD observed with total cells used at the beginning of the experiment. For RNS cells, neurospheres were obtained after culture and placed into slides in DMEM 10% FCS for 24 hours. Neurospheres adhesion was evaluated by counting the percentage of adherent neurospheres. These assays were performed in the absence or in the presence of 1 µM dasatinib.

Cell-cell adhesion assay - Spheroid formation experiments were performed by incubating 5000 parental, controls and transfected U251 and U87 cells per well in a 96-well plate previously coated with 75 µl of 1.5% agar gel. Images were taken after 72 hours and spheroid density was estimated using ImageJ by calculating the spheres' size. High spheres' size corresponds to the lower cell-cell adhesion. These assays were performed in the absence or in the presence of 1 µM dasatinib.

Boyden chamber migration assay - Parental, controls and transfected U251 and U87 cell lines were washed in DMEM, placed in Boyden chambers (10⁵ cells/chamber in DMEM) that were placed in DMEM 20% FBS and incubated at 37°C for 24 hours. After 24 hours, Boyden chambers were washed in PBS and cells were fixed in PBS 0.5% paraformaldehyde. For RNS

cell migration, Boyden chambers were previously coated with collagen (400 µg/ml) overnight. Non-migrated cells inside the chambers were removed and cells were then stained with Giemsa (RAL Diagnostics, Martillac, France). After washes in PBS, pictures of 5 different fields were taken. Migration was given by the mean of number of migrated cells observed per field. For inhibition with chemical drugs, cells were pre-incubated 15 minutes with SRC family kinases inhibitors PP2 (Sigma-Aldrich; 10 µM) and dasatinib (1 µM); ROCK inhibitor Y27632 (Selleckchem) and with FAK inhibitor Y15 (Sigma-Aldrich; 1 µM). Kinases inhibitors were kept during the time of migration assay. For migration of CD90^{high} RNS cell lines in the presence of dasatinib, values of migration were corrected by a factor of 1.15 due to the fact that viability of these cells were affected by this inhibitor (10 to 20% of cell death).

MRI analysis - Eighty-nine treatment-naive GBM patients (males: n=59; females: n=30; median age = 59 years - from 14 to 89 years) from the Cancer Genome Atlas (TCGA) cohort were analyzed for CD90 expression from transcriptome data and corresponding pretreatment MRI imaging data. The images were downloaded from the NCI's The Cancer Imaging Archive (TCIA) (<http://cancerimagingarchive.net/>). Preoperative qualitative and semi-quantitative imaging variables were provided by the Visually Accessible Rembrandt Images (VASARI) feature set (32). Details of the imaging variables and acquisition were published previously (33, 34). Medians of the CD90 mRNA expression level between each VASARI feature were compared using the Mann-Whitney test. Kaplan-Meier analysis was used to estimate the survival difference between different imaging features. For animal experiments, untreated mice bearing parental U87 (n=1) or U87 CD90 cells (n=4), and dasatinib-treated mice bearing U87 CD90 cells (n=4) were analyzed by MRI as previously described (35). Briefly, MRI acquisitions were performed on a horizontal 4.7 T Bruker Biospec 47/40 magnet interfaced to an AVANCE console (Bruker BioSpin, Ettlingen, Germany) and a workstation running the ParaVision 5.1

software. A linear-volume radio frequency coil (72 mm inner diameter) was used as transmitter and a home-made surface radio frequency coil (15 mm diameter) was used as receiver. The anesthesia was induced with 3% of isoflurane in 0.5L/min of air. The mice were positioned in a MRI compatible stereotactic holder to maintain the head fixed using ear bars a nose bar. Brain lesion was assessed using T2-weighted images obtained using a rapid acquisition with relaxation enhancement (RARE) as described in (36) with the following acquisition parameters: TR=3500 ms, TE=32.1 ms, RARE factor=8. Nine to eleven contiguous slices of 750 μ m were acquired to cover the whole brain.

Statistics - Values represent the mean \pm SD of n different experiments. Student t-test was applied using a two-tailed distribution of two conditions of unequal or equal variances on groups of data obtained in experiments. ANOVA method was used for comparing multiple conditions. These analyses were performed with GraphPad Prism software (La Jolla, United-States of America). The significance level was $p < 0.05$.

RESULTS

CD90 is expressed on CD133 positive and stem and non-stem GBM cells.

CD90 has been initially described in GBM specimens (5) and immortalized glioma/GBM cell lines (6-10), but is currently considered as a human GSC marker (11-15). CD90 is also found in GASCs (16) and mesenchymal stem cell-like pericytes (17). However, we observed expression of CD90 in human adherent primary GBM cells, which do not display stem-like characteristics. To clarify this discrepancy, CD90 mRNA expression was analyzed in primary GBM stem-like cells (RNS, n=12) that were previously characterized by us in (23); and in adherent cells (RADH, n=5) using transcriptome data (22, 23). Both CD133^{high} and CD133^{low} RNS cells, RADH cells and GBM samples (n=4) expressed high levels of CD90 mRNA (Figure 1A). Interestingly, CD90 transcripts were also observed in the NCI brain-derived cell lines panel (26) (Figure S1A), in both adherent and GSC lines (27) (Figure S1B), and finally in high-grade gliomas and GBM tumor specimens (28-31) (Figures S1B and S1C).

CD90 protein expression was studied using flow cytometry in primary RNS and RADH cells and in U251 and U87 cell lines (Figures 1B and S2A). All the primary cells (i.e. CD133^{high} RNS (n=6), CD133^{low} RNS (n=6), RADH (n=11)) and U251 cells expressed CD90 at high levels with a stronger expression observed on RADH and U251 cells (Figures 1B and S2A). In contrast, U87 cells did not express CD90 (Figure S2A). Interestingly, correlation between CD90 mRNA and protein expression was observed using RNS cell lines (Figure S2D). The analysis of dissociated GBM samples (n=36) revealed that CD90 was expressed in most GBM specimens tested (34 out of 36) (Figures 1C, S2B and S2C) with various intensities (~ 3 logs variation of specific fluorescence intensity) (Figure 1C). CD90 expression was confirmed using immunohistochemistry on high (GBM#179) and intermediate (GBM#217) CD90 expressing specimens with a clear staining in both tumor cells and on blood vessels (Figure 1D). A staining restricted to the vessels was only observed in CD90^{low} tumors (GBM#233) (Figure 1D). CD90

expression was also observed in xenografts obtained after injection with GBM primary cell lines, although inconsistent CD90 immunostaining was observed (Figure S2E). To further confirm that CD90 was expressed selectively in tumor cells, double staining with antibodies against CD90 and tumor (IL13R α 2, (37)), neural (CD200), endothelial (CD31) or stem (CD133) markers were performed in 8 GBM specimens and their peritumoral counterparts using flow cytometry (Figures 1E, S2F and S2G). Most of the CD90 positive cells from GBM were also positive for IL13R α 2 (69% in average). In contrast, most of the CD90 positive cells found in peritumoral tissues co-expressed CD200 (74% in average), a neural marker. A small fraction of CD90+ cells also expressed either CD31 or CD133 only in GBM samples indicating that endothelial and GBM stem cells within the tumor also expressed CD90 (respectively 15 and 6% in average). Other brain cell types such as astrocytes and pericytes could also express CD90, but were not identified using our experimental settings. These results indicate that CD90 expression varies between GBM patients is not restricted to CD133^{high} stem-like GBM cells but is also found in CD133^{low} stem-like GBM cells as well as in more differentiated tumor cells.

CD90 is associated with a cell adhesion/migration gene signature and invasive tumors in GBM patients.

To better characterize the role of CD90 in GBM, gene expression profiling was performed on an in-house cohort of 77 GBM specimens (Table S1) and analyzed in regards to CD90 expression. To this end, two groups of 16 GBM patients were defined according to CD90 expression in the microarray data with CD90^{low} patients exhibiting a CD90 expression value lower than the 20th percentile of the CD90 expression distribution, and CD90^{high} patients with a CD90 expression value higher than the 80th percentile of the CD90 expression distribution (Figure 2A). Differential gene expression profiling revealed that CD90^{high} tumors also exhibited a cell adhesion/migration gene signature comprising a highly connected gene network (Figure 2B and

Tables S2 to S4). Interestingly, genes found in the adhesion/migration signature such as collagens and PDGFRB were also over-expressed in CD90^{high} RNS cell lines (Figure S3A). The expression of CD90 mRNA was also highly expressed in mesenchymal and classical GBM subtypes previously described by Verhaark *et al.* (Figure 2C) (38). In addition, CD90^{high} tumors exhibited characteristic features of Epithelial-to-Mesenchymal Transition (EMT) as indicated by the up-regulation of α SMA, collagens (COL1A1, COL1A2 and COL5A2), metalloproteinases (MMP-2 and -9) (Figure S3B) and the transcription factors FOXC, GSC, SNAI2, TWIST-1 and -2 (Figure S3C). Furthermore, other mesenchymal markers such as cadherins were also overexpressed in CD90^{high} tumors (Figure S3D) while epithelial markers were expressed at similar levels in both CD90^{low} and CD90^{high} groups (Figure S3E). These results show that CD90 expression is linked to a cell adhesion/migration and EMT-linked gene signatures in GBM patients. Our data were then correlated to those relative to images from patients' tumors within the TCGA GBM cohort (32). Indeed, the Visually Accessible Rembrandt Images (VASARI) feature set was applied in the imaging assessments and analysis of 89 GBM patients from the TCGA GBM cohort (33, 34); and tested for associations with CD90 expression. Among all VASARI imaging features, CD90 mRNA expression level was significantly different in those patients with non-enhancing tumor crossing midline versus those not crossing midline; and in patients with multifocal/multicentric versus focal tumors (Figures 2E and 2F). Interestingly these imaging features were linked previously to an invasive profile revealed in patients with shorter survival and specific tumor gene signature associated with mitochondrial dysfunction (34). These data demonstrate that CD90 expression in tumor cells is associated also with a more invasive tumor phenotype.

Modulation of CD90 expression affects cell-cell/matrix adhesion and migration of GBM cells in vitro.

To study the role of CD90 in GBM cells, CD90 was either silenced in CD90 positive U251 cells or re-expressed in CD90 negative U87 cells. Silencing efficiency was verified using both flow cytometry (Figures S4A and S4B) and Western blot (Figure S4C). Cell viability and proliferation were not affected by CD90 modulation when compared to parental or mock-transfected cell lines over 5 days (Figures S4D and S4E). Cell-cell adhesion properties were tested in a spheroid formation assay using both U251 and U87 cells. CD90^{high} U251 cells formed spheroids less compact than those formed by CD90^{low} U251 cells and CD90 negative U87 cells (Figures S4F and S4G) suggesting that high CD90 expression could alter cell-cell adhesion. In contrast, cell adhesion to collagen was reduced when CD90 expression was decreased in U251 cells (Figure 3H), whereas no significant effect was observed with U87 cells, which present a strong collagen-cell interaction unrelated to CD90 expression (Figure 3H). Overall, these data indicate that CD90 limits cell-cell adhesion and increases cell-matrix adhesion ability of GBM cells. Cell migration was then evaluated using both wound healing- (Figures S5A and S5B) and Boyden chamber- (Figures 3A and 3B) based migration assays. In both cases, decreased CD90 expression in U251 cells reduced migration and re-expression of CD90 in U87 increased migration. Similarly, CD90^{high} GBM primary lines exhibited stronger migration indexes than their CD90^{low} counterparts (Figures 3C and 3D). Furthermore, shRNA-mediated silencing of CD90 in CD90^{high} primary GBM lines (Figures S5C and S5D) dramatically reduced cell migration (Figures 3E and S5E). Overall, these results show that CD90 expression is involved in GBM cell adhesion/migration properties.

CD90 expression affects GBM tumor shape in mice.

Parental and CD90 expressing U87 cells were tested for their tumorigenicity in an orthotopic xenograft mouse model. Most of the mice bearing parental U87 cells developed a clear encapsulated tumor mass 28 days post-injection that was evaluated using both MRI (Figure 3E;

n=1) and H&E staining of brain sections (Figure 3F; n=5 out of 7). Tumor formation was not detected in mice injected with U87 CD90 cells using MRI (Figure 3E; n=4). However, H&E staining revealed the presence of tumors with an irregular/invasive shape in mice injected with U87 CD90 cells (n=5 out of 7) whereas mice injected with parental U87 cells displayed encapsulated tumors with regular edges (Figure 3F). Moreover, serial H&E sections revealed the presence of the U87 CD90 tumor mass at a distance from the injection site, indicating its invasive feature (Figures 3G and 3H). Furthermore, CD90^{low} and CD90^{high} expressing RNS cells (n=2 and 4, respectively) were used in an orthotopic xenograft mouse model. Clinical signs appeared between 76 and 140 days post-implantation, depending on the cell line but independent on CD90 expression. Massive tumor infiltration within the brain parenchyma was observed with CD90^{high} RNS cells contrasting with a more limited invasion observed with CD90^{low} RNS cells (Figures 3I and 3J). These data are consistent with the results obtained in patients from the TCGA cohort and demonstrate that CD90 expression in tumor cells is associated with a more invasive tumor phenotype.

CD90 signals through SRC and FAK.

To investigate CD90-dependent signaling, U251 shCD90 and U87 CD90 transfectants were analyzed for total phosphotyrosine containing proteins using Western blot in comparison to parental and U251 shCTR and U87 CTR cells, respectively (Figure 4A). Phosphotyrosine signal increase was observed in U87 CD90^{high} cells compared to the parental cells which was confirmed in U251 cells with an observed decrease of phosphotyrosine containing proteins in U251 shCD90 (Figure 4A). FAK and SRC kinases were previously described to transduce CD90 signals (39, 40) and total SRC and FAK did not vary in CD90^{high} and CD90^{low} cell lines (Figure 4A). However, increase in SRC and FAK tyrosine phosphorylation was observed in U87 CD90^{high} cells (Figures 4A and 4B). In contrast, a decrease in SRC and FAK phosphorylation

was observed with U251 silenced for CD90. The expression levels of other SFK family members including FYN, LCK and YES1 was high in primary GBM cell lines (Figure S6A) and GBM patients' specimens (Figure S6B), with a significant increase of FYN mRNA expression in CD90^{high} patients. However, no difference in SRC and FAK expression at the protein level was observed in CD90^{low} and CD90^{high} primary cells (Figures S6C and S6D). Finally, increased phosphorylation of SRC and FAK was observed in CD90^{high} primary GBM cells compared to CD90^{low} primary cells (Figure 4C). Remarkably, FAK tyrosine phosphorylation was stronger in RADH lines compared to RNS lines, whereas no difference linked to culture conditions was observed regarding SRC tyrosine phosphorylation. To further document SRC activation in CD90^{low} and CD90^{high} primary GBM cell lines and in GBM patients' tumors, the SRC gene signature established by Bild *et al.* (41) was used to score SRC activation. Interestingly, SRC activation was predominantly associated with high CD90 expression in primary GBM cell lines (Figure 4D). However, using the same approach, high SRC activation was found in GBM tumors independent of CD90 expression (Figure S6E). This was possibly due to the high cellular heterogeneity and to the complex stroma of those tumors. To further investigate this observation in GBM tumors, freshly dissociated GBM specimens were tested for the presence of CD90 and phosphoSRC using flow cytometry. High levels of SRC phosphorylation correlated with high CD90 expression in GBM specimens (Figures 4E and 4F). Importantly, pre-treatment of GBM cells with dasatinib, a SRC inhibitor, blunted SRC phosphorylation (Figure S6F). These data indicated that high CD90 expression correlates with the activation of SRC signaling in GBM tumor cells.

CD90-mediated migration is dependent on SRC activation.

To confirm the impact of CD90-dependent signaling on cell migration in U251 and U87 cells, the chemical SRC inhibitors PP2 and dasatinib, the FAK inhibitor Y15 and the ROCK inhibitor

Y27632 were tested in Boyden chamber migration assays using parental U251 and U87 CD90 cells (Figure 5A). These inhibitors had no effect on cell viability during the time of the assay (Figure S7A). The SRC family kinases inhibitors PP2 and dasatinib dramatically reduced U251 and U87 CD90 migration. Migration inhibition was also observed upon treatment with the ROCK inhibitor Y27632 (53% and 76% reduction using U251 and U87 CD90 cells respectively) but to a lesser extent. In contrast, the FAK inhibitor Y15 had no or limited effect on the migration of U251 and U87 CD90 cells. Interestingly, dasatinib also dramatically reduced the migration of primary CD90^{high} GBM lines (Figures 5B and 5C). These results indicate that CD90-mediated migration mainly depends on the SRC family kinases, and to a lesser extent of ROCK and FAK. Inhibitors of downstream signals such as Rac1, MEK1 and JNK also affected the migration of CD90^{high} cells (Figure S7B).

Dasatinib inhibits CD90-mediated migration of GBM cells in vivo.

To evaluate the CD90-dependent effects of dasatinib *in vivo*, U87 CD90 cells were used in an orthotopic xenograft mouse model. One week post-implantation, mice were treated with dasatinib (40 mg/kg) for 20 days. Mice were then analyzed using MRI 28 days post-injection and were sacrificed. As observed previously (Figures 3E and 3F), U87 CD90 injected mice did not revealed any MRI-detectable tumors (Figure 5D, n=4) whereas an irregular tumor mass was observed after H&E staining (Figure 5E, n=6 out of 7). In contrast, small but clear encapsulated tumors with regular edges were observed using both MRI (Figure 5D, n=3 out of 4) and H&E staining (Figure 5E, n=4 out of 7) in mice injected with U87 CD90 and treated with dasatinib. Again, serial H&E sections revealed a deep infiltration of U87 CD90 tumor cells within the parenchyma (up to 400 μ m away from the injection site), whereas very limited invasion was observed after dasatinib treatment (Figures 5F and 5E). These data demonstrate that dasatinib

attenuates CD90-dependent tumor migration/invasion properties *in vivo*, thus leading to smaller and less invasive tumors.

Dasatinib inhibits CD90-dependent cell/matrix adhesion.

To further investigate the effect of dasatinib on CD90-mediated GBM cell-matrix interaction, we first tested U87 CD90 and U251 cells both displaying strong collagen adherence properties. Dasatinib dramatically inhibited U87 CD90 and CD90^{low} U251 cells cell attachment to collagen (Figure 6A). We confirmed the effect of dasatinib on cell-matrix adhesion using primary RNS lines (enriched in stem cells) that were cultured under neurosphere conditions but had the unique property to partially adhere to the substrate, as previously described (42). Remarkably, CD90^{high} cells lost the ability to adhere to plastic upon dasatinib treatment whereas neurospheres derived from CD90^{low} cells remained adherent (Figures 6B and 6C). These results indicate that dasatinib modulates CD90-dependent cell/matrix adhesion properties of GBM cells.

CD90 expression levels predict GBM cell sensitivity to dasatinib.

As CD90 was considered as a GSC marker, we finally evaluated the impact of dasatinib on the viability of primary CD90^{low} and CD90^{high} RNS cells. Interestingly, CD90^{high} RNS cells were more sensitive to dasatinib than CD90^{low} RNS cells (IC50 in average 0.3 μ M versus 46.5 μ M respectively) (Figure 6D). Furthermore, the down-regulation of CD90 in CD90^{high} primary lines significantly reduced their sensitivity to dasatinib (Figure 6E). These data indicate that dasatinib affects the viability of CD90^{high} RNS cells enriched in GSCs.

CONCLUSION

In this study, we show that CD90 is expressed on both stem and differentiated GBM tumor cells, and we demonstrate that CD90 expression controls tumor cell migration/adhesion mainly through SRC signaling. In addition, we show that CD90 expression regulates tumor invasive characteristics in a mouse model and in human tumors. CD90 also regulates cell-cell/matrix adhesion properties of GBM cells. Finally, we provide evidence that dasatinib dramatically reduces CD90-mediated invasiveness of U87 CD90 cells in an orthotopic xenograft mouse model and that CD90 expression impacts on dasatinib sensitivity in patient-derived GSC lines. Collectively, this study unveils the importance of CD90 in GBM migration/invasion and points toward CD90 expression as a predictor of dasatinib response in GBM patients.

CD90 was described as a candidate marker for cancer stem cells from primary high-grade gliomas (11-15, 43). More recently, CD90 positive cells were also associated with blood vessels in human GBM tissues and characterized as immature mesenchymal stem cell-like pericytes (17). However, we observed that CD90 expression was high in human adherent primary GBM cells (22). High CD90 mRNA amounts were reported in established (26, 27) and primary (27) GBM cell lines as well as in tumor specimens (5, 28-31). To sort out this apparent discrepancy, we used flow cytometry and immunohistochemistry approaches in GBM samples, and we found that CD90 was highly expressed in endothelial cells within the tumor and on neurons present in the brain parenchyma as previously described (4, 19-21). We also observed CD90 expression in GBM derived stem and in more differentiated tumor cells using both cell lines and human tumor specimens.

One of the important features of GBM is the diffuse invasion of tumor cells within the surrounding brain parenchyma (44), thus rendering complete surgical resection impossible (45, 46). We showed that U87- or RNS-derived CD90^{high} tumors displayed a more invasive phenotype in an orthotopic mouse model compared to their CD90^{low} counterparts. This

observation correlated with patients' data since CD90^{high} tumors also presented invasive imaging features. Interestingly these invasive features were previously linked to other gene signatures including mitochondrial dysfunction and remodelling of epithelial adherens junctions; and displayed shorter patients' survival (34). The CD90-dependent invasive characteristics of GBM cells were then correlated to gene expression and signaling data. Interestingly, CD90^{high} GBM were characterized by an adhesion/migration gene signature and were enriched in GBM mesenchymal type, exhibiting elevated expression of mesenchymal markers such as α SMA, COL1A1, COL1A2 and MMP-2 and -9. Overexpression of these specific genes could be related to the increased invasiveness observed in CD90^{high} tumors and linked CD90-dependent signaling through p100, CD45, the SRC family kinases (SFK) LYN and FYN and small G proteins (18-21). CD90 also regulates actin and tubulin cytoskeleton reorganisation, focal disassembly, leading to modulation of cell migration (19, 20). In the present study, we demonstrate that CD90 controls GBM cell migration/invasion mainly through SRC signaling. SRC and c-YES kinases have been recently involved in migration of glioma stem cells (47). The relevance of SRC signaling was confirmed by the identification of a SRC gene signature (41) in CD90^{high} GBM primary cell lines compared to their CD90^{low} counterparts. Furthermore, increased SRC phosphorylation was observed in freshly dissociated CD90^{high} GBM tumors. Interestingly SRC phosphorylation has previously been observed in GBM cells of the center and the borders of the tumor site as well as in invasive tumor cells within the brain parenchyma (48, 49). We cannot presently completely rule out that other SFK family members might also be involved. However, we did not observe any c-YES activation in U251 and U87 cells modified for CD90 expression. Only a significant increase of FYN mRNA expression was also observed in CD90^{high} patients.

In the past few years, intensive research programs have identified new therapeutic agents that target glioma migration/invasion (45, 46). For instance inhibition of metalloproteinases (50-52), blockade of integrins (53-55), targeting of cytoskeleton reorganization (56) and inhibition of

signaling molecules such as FAK (57-59) and SFK (48, 60-62) showed promising effects on GBM invasiveness *in vitro* and GBM progression in mouse models (45, 46). Some of these molecules have also been used in recent GBM clinical trials. As such marimastat, a MMP inhibitor, showed encouraging effects on recurrent GBM patients (63) but failed to improve patient survival in a phase III clinical trial (64). Cilengitide, a $\alpha v\beta 3$ and $\alpha v\beta 5$ -integrins antagonist, combined with temozolomide showed limited effects on GBM patients (65). Dasatinib showed promising effect on inhibiting bevacizumab-induced glioma cell invasion at a preclinical stage (62), but failed to improve bevacizumab-treated recurrent GBM patients in a phase II trial (66). Interestingly, SFK family kinases including SRC, FYN, and c-YES are involved in glioma proliferation and motility *in vitro* (67). LYN and c-YES have opposite effects on survival in a glioma orthotopic xenograft model. Here we show that dasatinib affects the viability of CD90^{high} RNS cells and blocks CD90-dependent GBM migration *in vivo*. We propose a model that defines the rational for using dasatinib in CD90^{high} GBM patients by targeting both GSC proliferation and GBM cells migration/invasion (Figure 6F). Our results strongly emphasize the need of re-addressing dasatinib response in GBM patients following a CD90-based stratification This type of approach could for instance be completely applicable for plurilobar GBM tumors (i.e. that can neither be resected nor irradiated, as observed in the multifocal/multicentric group from the TCGA cohort).

In conclusion, our data point towards CD90 as a marker of tumor invasion and might also be considered as a GBM stratification tool for clinical trials testing new therapeutic agents that target SRC-dependent GBM migration/invasion. Our results also pave the way for novel therapeutic approaches targeting CD90 and its downstream signaling to be applied to GBM patients.

REFERENCES

1. Cloughesy TF, Cavenee WK, Mischel PS. Glioblastoma: from molecular pathology to targeted treatment. *Annual review of pathology*. 2014;9:1-25.
2. Weathers SP, Gilbert MR. Advances in treating glioblastoma. *F1000prime reports*. 2014;6:46.
3. Huse JT, Holland E, DeAngelis LM. Glioblastoma: molecular analysis and clinical implications. *Annual review of medicine*. 2013;64:59-70.
4. Bradley JE, Ramirez G, Hagood JS. Roles and regulation of Thy-1, a context-dependent modulator of cell phenotype. *BioFactors*. 2009;35(3):258-65.
5. Wikstrand CJ, Grahmann FC, McComb RD, Bigner DD. Antigenic heterogeneity of human anaplastic gliomas and glioma-derived cell lines defined by monoclonal antibodies. *Journal of neuropathology and experimental neurology*. 1985;44(3):229-41.
6. Kemshead JT, Ritter MA, Cotmore SF, Greaves MF. Human Thy-1: expression on the cell surface of neuronal and glial cells. *Brain research*. 1982;236(2):451-61.
7. Hurwitz E, Arnon R, Sahar E, Danon Y. A conjugate of adriamycin and monoclonal antibodies to Thy-1 antigen inhibits human neuroblastoma cells in vitro. *Annals of the New York Academy of Sciences*. 1983;417:125-36.
8. Seeger RC, Danon YL, Rayner SA, Hoover F. Definition of a Thy-1 determinant on human neuroblastoma, glioma, sarcoma, and teratoma cells with a monoclonal antibody. *Journal of immunology*. 1982;128(2):983-9.
9. Wikstrand CJ, Bigner SH, Bigner DD. Demonstration of complex antigenic heterogeneity in a human glioma cell line and eight derived clones by specific monoclonal antibodies. *Cancer research*. 1983;43(7):3327-34.
10. Rettig WJ, Chesa PG, Beresford HR, Feickert HJ, Jennings MT, Cohen J, et al. Differential expression of cell surface antigens and glial fibrillary acidic protein in human astrocytoma subsets. *Cancer research*. 1986;46(12 Pt 1):6406-12.
11. He J, Liu Y, Zhu T, Zhu J, Dimeco F, Vescovi AL, et al. CD90 is identified as a candidate marker for cancer stem cells in primary high-grade gliomas using tissue microarrays. *Molecular & cellular proteomics : MCP*. 2012;11(6):M111 010744.
12. Kang MK, Kang SK. Tumorigenesis of chemotherapeutic drug-resistant cancer stem-like cells in brain glioma. *Stem cells and development*. 2007;16(5):837-47.
13. Tomuleasa C, Soritau O, Rus-Ciuca D, Ioani H, Susman S, Petrescu M, et al. Functional and molecular characterization of glioblastoma multiforme-derived cancer stem cells. *J BUON*. 2010;15(3):583-91.
14. Liu G, Yuan X, Zeng Z, Tunici P, Ng H, Abdulkadir IR, et al. Analysis of gene expression and chemoresistance of CD133+ cancer stem cells in glioblastoma. *Molecular cancer*. 2006;5:67.
15. Nitta RT, Gholamin S, Feroze AH, Agarwal M, Cheshier SH, Mitra SS, et al. Casein kinase 2alpha regulates glioblastoma brain tumor-initiating cell growth through the beta-catenin pathway. *Oncogene*. 2015;34(28):3688-99.
16. Clavreul A, Etcheverry A, Chassevent A, Quillien V, Avril T, Jourdan ML, et al. Isolation of a new cell population in the glioblastoma microenvironment. *Journal of neuro-oncology*. 2012;106(3):493-504.
17. Ochs K, Sahm F, Opitz CA, Lanz TV, Oezen I, Couraud PO, et al. Immature mesenchymal stem cell-like pericytes as mediators of immunosuppression in human malignant glioma. *Journal of neuroimmunology*. 2013;265(1-2):106-16.
18. Haeryfar SM, Hoskin DW. Thy-1: more than a mouse pan-T cell marker. *Journal of immunology*. 2004;173(6):3581-8.

19. Rege TA, Hagood JS. Thy-1 as a regulator of cell-cell and cell-matrix interactions in axon regeneration, apoptosis, adhesion, migration, cancer, and fibrosis. *FASEB journal : official publication of the Federation of American Societies for Experimental Biology*. 2006;20(8):1045-54.
20. Barker TH, Hagood JS. Getting a grip on Thy-1 signaling. *Biochimica et biophysica acta*. 2009;1793(5):921-3.
21. Leyton L, Hagood JS. Thy-1 modulates neurological cell-cell and cell-matrix interactions through multiple molecular interactions. *Advances in neurobiology*. 2014;8:3-20.
22. Avril T, Saikali S, Vauleon E, Jary A, Hamlat A, De Tayrac M, et al. Distinct effects of human glioblastoma immunoregulatory molecules programmed cell death ligand-1 (PDL-1) and indoleamine 2,3-dioxygenase (IDO) on tumour-specific T cell functions. *Journal of neuroimmunology*. 2010;225(1-2):22-33.
23. Avril T, Vauleon E, Hamlat A, Saikali S, Etcheverry A, Delmas C, et al. Human glioblastoma stem-like cells are more sensitive to allogeneic NK and T cell-mediated killing compared with serum-cultured glioblastoma cells. *Brain pathology*. 2012;22(2):159-74.
24. Drogat B, Auguste P, Nguyen DT, Bouchecareilh M, Pineau R, Nalbantoglu J, et al. IRE1 signaling is essential for ischemia-induced vascular endothelial growth factor-A expression and contributes to angiogenesis and tumor growth in vivo. *Cancer research*. 2007;67(14):6700-7.
25. Schneider CA, Rasband WS, Eliceiri KW. NIH Image to ImageJ: 25 years of image analysis. *Nature methods*. 2012;9(7):671-5.
26. Pfister TD, Reinhold WC, Agama K, Gupta S, Khin SA, Kinders RJ, et al. Topoisomerase I levels in the NCI-60 cancer cell line panel determined by validated ELISA and microarray analysis and correlation with indenoisoquinoline sensitivity. *Molecular cancer therapeutics*. 2009;8(7):1878-84.
27. Schulte A, Gunther HS, Phillips HS, Kemming D, Martens T, Kharbanda S, et al. A distinct subset of glioma cell lines with stem cell-like properties reflects the transcriptional phenotype of glioblastomas and overexpresses CXCR4 as therapeutic target. *Glia*. 2011;59(4):590-602.
28. Phillips HS, Kharbanda S, Chen R, Forrest WF, Soriano RH, Wu TD, et al. Molecular subclasses of high-grade glioma predict prognosis, delineate a pattern of disease progression, and resemble stages in neurogenesis. *Cancer cell*. 2006;9(3):157-73.
29. Freije WA, Castro-Vargas FE, Fang Z, Horvath S, Cloughesy T, Liau LM, et al. Gene expression profiling of gliomas strongly predicts survival. *Cancer research*. 2004;64(18):6503-10.
30. Donson AM, Birks DK, Schittone SA, Kleinschmidt-DeMasters BK, Sun DY, Hemenway MF, et al. Increased immune gene expression and immune cell infiltration in high-grade astrocytoma distinguish long-term from short-term survivors. *Journal of immunology*. 2012;189(4):1920-7.
31. Sturm D, Witt H, Hovestadt V, Khuong-Quang DA, Jones DT, Konermann C, et al. Hotspot mutations in H3F3A and IDH1 define distinct epigenetic and biological subgroups of glioblastoma. *Cancer cell*. 2012;22(4):425-37.
32. Mazurowski MA, Desjardins A, Malof JM. Imaging descriptors improve the predictive power of survival models for glioblastoma patients. *Neuro-oncology*. 2013;15(10):1389-94.
33. Zinn PO, Mahajan B, Sathyan P, Singh SK, Majumder S, Jolesz FA, et al. Radiogenomic mapping of edema/cellular invasion MRI-phenotypes in glioblastoma multiforme. *PloS one*. 2011;6(10):e25451.
34. Colen RR, Vangel M, Wang J, Gutman DA, Hwang SN, Wintermark M, et al. Imaging genomic mapping of an invasive MRI phenotype predicts patient outcome and metabolic dysfunction: a TCGA glioma phenotype research group project. *BMC medical genomics*. 2014;7:30.

35. Dietrich Y, Eliat PA, Dieuset G, Saint-Jalmes H, Pineau C, Wendling F, et al. Structural and functional changes during epileptogenesis in the mouse model of medial temporal lobe epilepsy. Conference proceedings : Annual International Conference of the IEEE Engineering in Medicine and Biology Society IEEE Engineering in Medicine and Biology Society Annual Conference. 2016;2016:4005-8.
36. Hennig J, Nauerth A, Friedburg H. RARE imaging: a fast imaging method for clinical MR. *Magnetic resonance in medicine*. 1986;3(6):823-33.
37. Saikali S, Avril T, Collet B, Hamlat A, Bansard JY, Drenou B, et al. Expression of nine tumour antigens in a series of human glioblastoma multiforme: interest of EGFRvIII, IL-13Ralpha2, gp100 and TRP-2 for immunotherapy. *Journal of neuro-oncology*. 2007;81(2):139-48.
38. Verhaak RG, Hoadley KA, Purdom E, Wang V, Qi Y, Wilkerson MD, et al. Integrated genomic analysis identifies clinically relevant subtypes of glioblastoma characterized by abnormalities in PDGFRA, IDH1, EGFR, and NF1. *Cancer cell*. 2010;17(1):98-110.
39. Rege TA, Pallero MA, Gomez C, Grenett HE, Murphy-Ullrich JE, Hagood JS. Thy-1, via its GPI anchor, modulates Src family kinase and focal adhesion kinase phosphorylation and subcellular localization, and fibroblast migration, in response to thrombospondin-1/hep I. *Experimental cell research*. 2006;312(19):3752-67.
40. Barker TH, Pallero MA, MacEwen MW, Tilden SG, Woods A, Murphy-Ullrich JE, et al. Thrombospondin-1-induced focal adhesion disassembly in fibroblasts requires Thy-1 surface expression, lipid raft integrity, and Src activation. *The Journal of biological chemistry*. 2004;279(22):23510-6.
41. Bild AH, Yao G, Chang JT, Wang Q, Potti A, Chasse D, et al. Oncogenic pathway signatures in human cancers as a guide to targeted therapies. *Nature*. 2006;439(7074):353-7.
42. Lottaz C, Beier D, Meyer K, Kumar P, Hermann A, Schwarz J, et al. Transcriptional profiles of CD133+ and CD133- glioblastoma-derived cancer stem cell lines suggest different cells of origin. *Cancer research*. 2010;70(5):2030-40.
43. He J, Liu Y, Xie X, Zhu T, Soules M, DiMeco F, et al. Identification of cell surface glycoprotein markers for glioblastoma-derived stem-like cells using a lectin microarray and LC-MS/MS approach. *Journal of proteome research*. 2010;9(5):2565-72.
44. Louis DN, Ohgaki H, Wiestler OD, Cavenee WK, Burger PC, Jouvet A, et al. The 2007 WHO classification of tumours of the central nervous system. *Acta neuropathologica*. 2007;114(2):97-109.
45. Zhong J, Paul A, Kellie SJ, O'Neill GM. Mesenchymal migration as a therapeutic target in glioblastoma. *Journal of oncology*. 2010;2010:430142.
46. Vehlow A, Cordes N. Invasion as target for therapy of glioblastoma multiforme. *Biochimica et biophysica acta*. 2013;1836(2):236-44.
47. Han X, Zhang W, Yang X, Wheeler CG, Langford CP, Wu L, et al. The role of Src family kinases in growth and migration of glioma stem cells. *International journal of oncology*. 2014;45(1):302-10.
48. Lu KV, Zhu S, Cvrljevic A, Huang TT, Sarkaria S, Ahkavan D, et al. Fyn and SRC are effectors of oncogenic epidermal growth factor receptor signaling in glioblastoma patients. *Cancer research*. 2009;69(17):6889-98.
49. Feng H, Hu B, Jarzynka MJ, Li Y, Keezer S, Johns TG, et al. Phosphorylation of dedicator of cytokinesis 1 (Dock180) at tyrosine residue Y722 by Src family kinases mediates EGFRvIII-driven glioblastoma tumorigenesis. *Proceedings of the National Academy of Sciences of the United States of America*. 2012;109(8):3018-23.
50. Noha M, Yoshida D, Watanabe K, Teramoto A. Suppression of cell invasion on human malignant glioma cell lines by a novel matrix-metalloproteinase inhibitor SI-27: in vitro study. *Journal of neuro-oncology*. 2000;48(3):217-23.

51. Tonn JC, Kerkau S, Hanke A, Bouterfa H, Mueller JG, Wagner S, et al. Effect of synthetic matrix-metalloproteinase inhibitors on invasive capacity and proliferation of human malignant gliomas in vitro. *International journal of cancer Journal international du cancer*. 1999;80(5):764-72.
52. Price A, Shi Q, Morris D, Wilcox ME, Brasher PM, Rewcastle NB, et al. Marked inhibition of tumor growth in a malignant glioma tumor model by a novel synthetic matrix metalloproteinase inhibitor AG3340. *Clinical cancer research : an official journal of the American Association for Cancer Research*. 1999;5(4):845-54.
53. Yamada S, Bu XY, Khankaldyyan V, Gonzales-Gomez I, McComb JG, Laug WE. Effect of the angiogenesis inhibitor Cilengitide (EMD 121974) on glioblastoma growth in nude mice. *Neurosurgery*. 2006;59(6):1304-12; discussion 12.
54. Maurer GD, Tritschler I, Adams B, Tabatabai G, Wick W, Stupp R, et al. Cilengitide modulates attachment and viability of human glioma cells, but not sensitivity to irradiation or temozolomide in vitro. *Neuro-oncology*. 2009;11(6):747-56.
55. Mikkelsen T, Brodie C, Finnis S, Berens ME, Rennert JL, Nelson K, et al. Radiation sensitization of glioblastoma by cilengitide has unanticipated schedule-dependency. *International journal of cancer Journal international du cancer*. 2009;124(11):2719-27.
56. Yap CT, Simpson TI, Pratt T, Price DJ, Maciver SK. The motility of glioblastoma tumour cells is modulated by intracellular cofilin expression in a concentration-dependent manner. *Cell motility and the cytoskeleton*. 2005;60(3):153-65.
57. Shi Q, Hjelmeland AB, Keir ST, Song L, Wickman S, Jackson D, et al. A novel low-molecular weight inhibitor of focal adhesion kinase, TAE226, inhibits glioma growth. *Molecular carcinogenesis*. 2007;46(6):488-96.
58. Schultze A, Decker S, Otten J, Horst AK, Vohwinkel G, Schuch G, et al. TAE226-mediated inhibition of focal adhesion kinase interferes with tumor angiogenesis and vasculogenesis. *Investigational new drugs*. 2010;28(6):825-33.
59. Golubovskaya VM, Huang G, Ho B, Yemma M, Morrison CD, Lee J, et al. Pharmacologic blockade of FAK autophosphorylation decreases human glioblastoma tumor growth and synergizes with temozolomide. *Molecular cancer therapeutics*. 2013;12(2):162-72.
60. Angers-Loustau A, Hering R, Werbowetski TE, Kaplan DR, Del Maestro RF. SRC regulates actin dynamics and invasion of malignant glial cells in three dimensions. *Molecular cancer research : MCR*. 2004;2(11):595-605.
61. Milano V, Piao Y, LaFortune T, de Groot J. Dasatinib-induced autophagy is enhanced in combination with temozolomide in glioma. *Molecular cancer therapeutics*. 2009;8(2):394-406.
62. Huvelde D, Lewis-Tuffin LJ, Carlson BL, Schroeder MA, Rodriguez F, Giannini C, et al. Targeting Src family kinases inhibits bevacizumab-induced glioma cell invasion. *PloS one*. 2013;8(2):e56505.
63. Groves MD, Puduvalli VK, Hess KR, Jaeckle KA, Peterson P, Yung WK, et al. Phase II trial of temozolomide plus the matrix metalloproteinase inhibitor, marimastat, in recurrent and progressive glioblastoma multiforme. *Journal of clinical oncology : official journal of the American Society of Clinical Oncology*. 2002;20(5):1383-8.
64. Levin VA, Phuphanich S, Yung WK, Forsyth PA, Maestro RD, Perry JR, et al. Randomized, double-blind, placebo-controlled trial of marimastat in glioblastoma multiforme patients following surgery and irradiation. *Journal of neuro-oncology*. 2006;78(3):295-302.
65. Stupp R, Hegi ME, Gorlia T, Erridge SC, Perry J, Hong YK, et al. Cilengitide combined with standard treatment for patients with newly diagnosed glioblastoma with methylated MGMT promoter (CENTRIC EORTC 26071-22072 study): a multicentre, randomised, open-label, phase 3 trial. *The Lancet Oncology*. 2014;15(10):1100-8.

66. Lassman AB, Pugh SL, Gilbert MR, Aldape KD, Geinoz S, Beumer JH, et al. Phase 2 trial of dasatinib in target-selected patients with recurrent glioblastoma (RTOG 0627). *Neuro-oncology*. 2015;17(7):992-8.
67. Lewis-Tuffin LJ, Feathers R, Hari P, Durand N, Li Z, Rodriguez FJ, et al. Src family kinases differentially influence glioma growth and motility. *Molecular oncology*. 2015;9(9):1783-98.

CONFLICT OF INTEREST

The authors disclose no potential conflicts of interest.

ACKNOWLEDGMENTS

We thank Caroline Gouat and Ester Porée for their excellent technical assistance; Laurent Riffaud, Claire Haegelen and the medical staff of the Neurosurgery department at the CHU Pontchaillou (Rennes) for their contribution; Alain Fautrel and Pascale Bellaud from the Biosit histopathology H2P2 platform (Université de Rennes 1, France) for immunohistochemistry analyses on GBM specimens and tumor xenografts; the Biosit ARCHE animal facility (Université de Rennes 1) for animal housing; and Pierre-Antoine Eliat from the Biosit PRISM platform (Université de Rennes 1) for mouse MRI analyses.

FIGURE LEGENDS

Figure 1: *CD90 mRNA and protein are expressed on all GBM cells.* Total mRNA from CD133^{low} RNS (n=6; blank square), CD133^{high} RNS (n=6; blank square), RADH (n=5; black square) GBM cells and GBM specimens (n=4; black circle) was extracted and analyzed for a gene expression profile as described in (22, 23) (A). Results are expressed as fluorescence intensity levels observed in transcriptome microarrays. CD133^{low} RNS (n=6; blank square), CD133^{high} RNS (n=6; blank square), RADH (n=11; black square) GBM cells were stained with isotype controls or specific anti-CD90 antibodies and directly analyzed for CD90 protein expression by flow cytometry (B). Representative histograms are shown in supplementary data (Figure S2A). CD90 protein expression levels are expressed as the mean of specific fluorescence intensity of the protein expression determined in at least three different experiments as described in Materials and methods section. Human GBM specimens (n=36; black circle) were dissociated and analyzed for CD90 expression by flow cytometry (C) as described in (B). Representative histograms are shown in supplementary data (Figure S2B). Three corresponding tumor sections were analyzed by immunohistochemistry for CD90 protein expression (D). Tumor (black circle) and peritumoral (blank circle) specimens from the same GBM patient were analyzed for CD90 expression combined with a tumor (IL13R α 2), neural (CD200), endothelial (CD31) or stem cell (CD133) marker (n=8) (E). Gating strategies is presented in Figure S2F. Results are expressed as percentages of double positive cells within all samples. One GBM sample was negative for IL13R α 2 (dot in bracket). Representative histograms are shown in supplementary data (Figure S2G). (*): $p < 0.01$; (**): $p < 0.005$; (***): $p < 0,001$.

Figure 2: *CD90 expression is associated with a cell adhesion/migration gene signature and with multifocal/multicentric tumors in GBM patients.* Total mRNA from GBM specimens (n=77) was extracted and used for a gene expression profile by transcriptome microarray. GBM patients were divided into two distinct groups CD90^{low} (n=16, yellow) and CD90^{high} (n=16, blue) tumors according to their CD90 mRNA expression level (A). CD90^{low} (yellow) and CD90^{high} (blue) tumors were classified using hierarchical clustering method based on differentially expressed genes (56 and 368 probes highly expressed in CD90^{low} and CD90^{high} groups respectively) (A). Differential expressed genes were annotated using DAVID bioinformatics resources <http://david.ncifcrf.gov/>. A robust interconnected gene network is represented in a venn diagram with representative genes involved in cell adhesion and cell migration functions (B). GBM specimens were classified in the several GBM subtypes previously described by Verhaark *et al.* mRNA CD90 expression was then analyzed within these GBM subtypes (C). MRI of 89 GBM

patients from the TCGA dataset were analyzed according to VASARI features. Representative cases are shown in (E): tumors with (i, red arrows) and without (ii, blue arrows) crossing midline; multicentric tumors (iii, with two discrete foci shown by red arrows) and focal tumors (iv, blue arrows). CD90 mRNA expression levels were compared between different VASARI features and were statistically different in GBM patients with focal tumor versus multifocal/multicentric tumors and also in tumors with and without crossing midline (F). (*): $p < 0.05$; (**): $p < 0.01$; (***) : $p < 0.005$.

Figure 3: *CD90 affects migration of U251, U87 and GBM primary cells and is associated with invasive tumors in xenograft mouse model.* Parental (wt, blank), control (empty and shCTR#, n=2, grey), CD90-down expressing (shCD90#, n=3, yellow) U251 cells (A) ; as well as parental (wt, blank), control (CTR#, n=2, grey) and CD90 expressing (CD90#, n=3, blue) U87 cells (B); CD90^{low} (yellow) and CD90^{high} (blue) RNS (n=4, square) and RADH (n=4, circle) (C and D) cells were tested in a 24-hours Boyden chamber migration assay (A to D) as described in Materials and methods section. Representative fields are shown in (A and C). The migration index corresponded to the number of migrating cells obtained per field. Control sh#CTR (blue) and CD90-down expressing sh#CD90 (yellow) RNS (n=3, blank square) and RADH (n=3, blank circle) cells were tested in a 24-hours Boyden chamber migration assay (E) and representative fields are shown in Figure S5H. Parental and CD90-expressing U87 cells (E to H) or CD90^{low} and CD90^{high} RNS cells (I and J) were orthotopically implanted in immunocompromised mice brain. Mice bearing parental (n=1) and U87 CD90 (n=4) cells were analyzed using MRI (E) and sacrificed 28 days after injection; for RNS cells, mice were sacrificed when the clinical signs appeared. Brains were collected and sections were analyzed after H&E staining (F) or for vimentin expression by immunohistochemistry (I). Posterior section sides are shown in (F) for U87 cells and (I) for RNS cells. Serial sections (made every 50 μm) were prepared from the injection site (0 μm) and stained with H&E (G). The tumor shape was reconstituted using SketchUp (H). Tumor area was determined as described in Materials and methods section (J). (**): $p < 0.01$; (***) : $p < 0,001$.

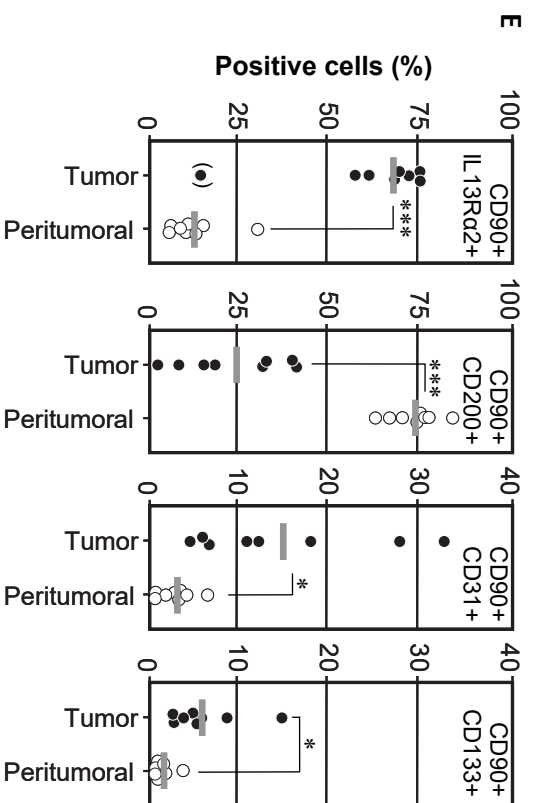
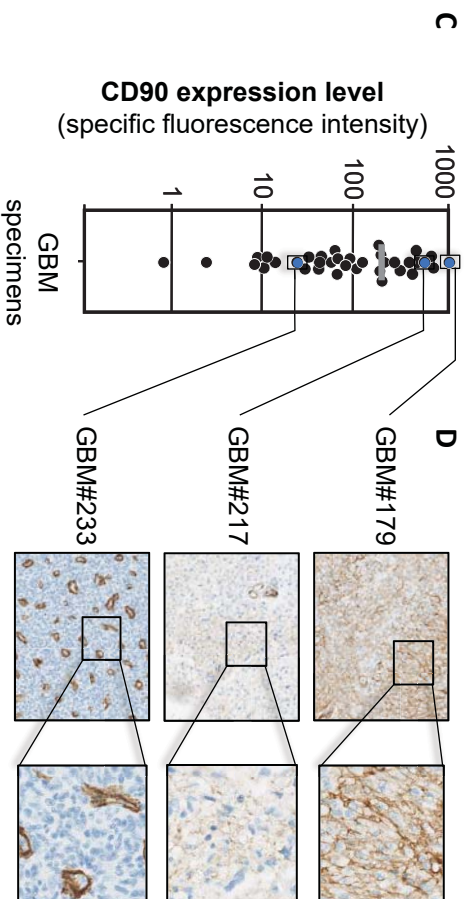
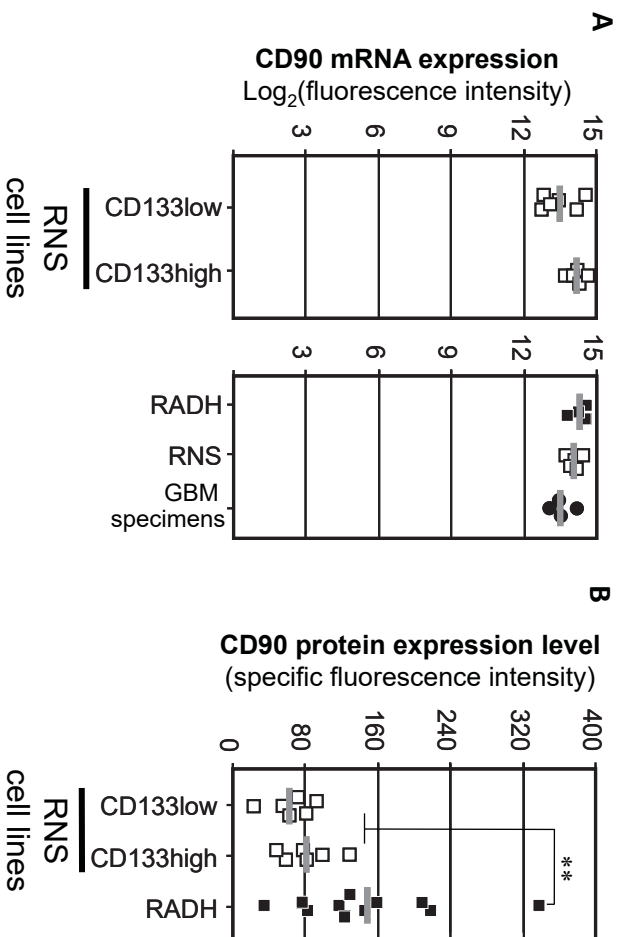
Figure 4: *CD90-dependent migration involves SRC and FAK kinases signaling.* Parental (wt, blank), control (shCTR#, grey), CD90-down expressing (shCD90#, n=3, yellow) U251 cells; as well as parental (wt, blank), control (CTR#, grey) and CD90 expressing (CD90#, n=3, blue) U87 cells were cultured at low cell density, lysed and analyzed by Western-blot for phosphotyrosine, phosphoSRC, SRC, phosphoFAK, FAK and β -actin expression (A). Arrowheads indicate

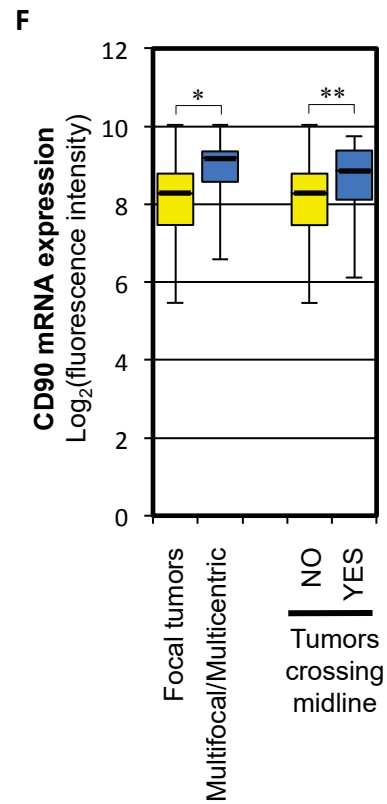
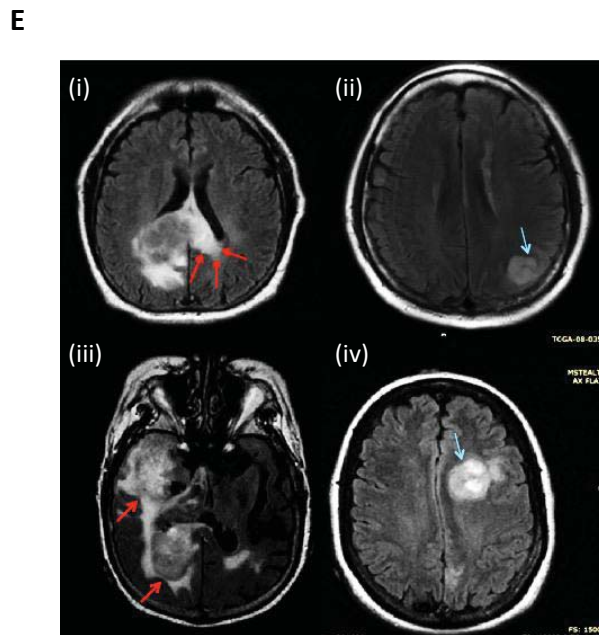
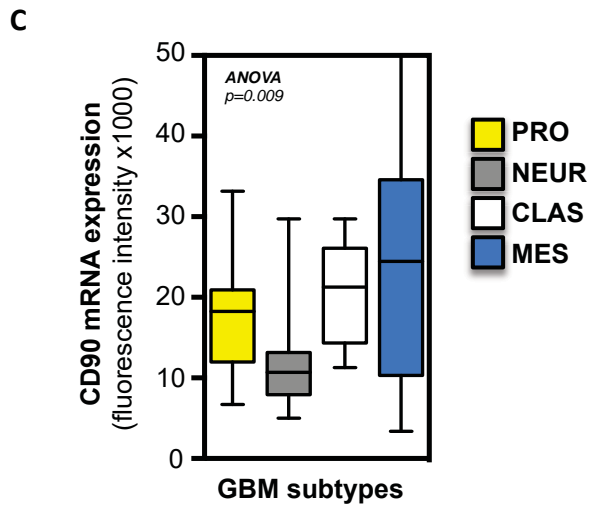
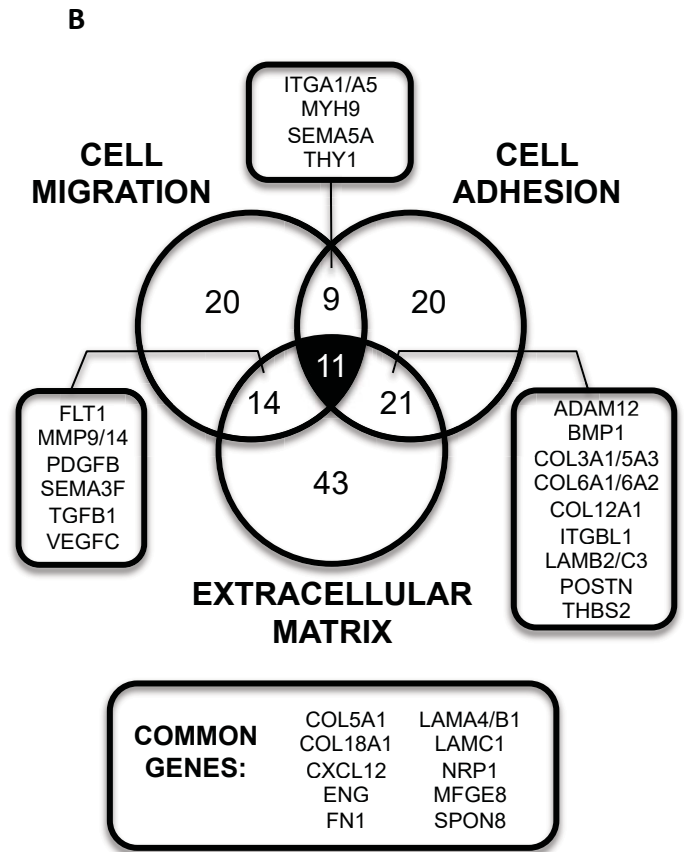
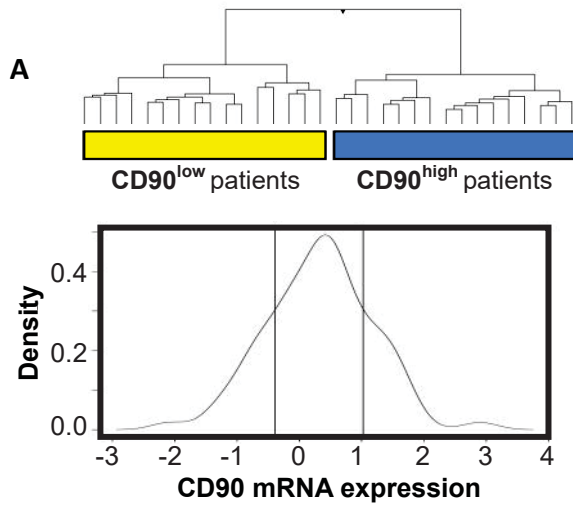
putative phosphorylated proteins associated with CD90 expression. Protein phosphorylation levels were calculated as described in Materials and Methods part (B). CD90^{low} (yellow) and CD90^{high} (blue) RNS (n=12, square) and RADH (n=6, circle) cells were analyzed by Western-blot for phosphoSRC, SRC, phosphoFAK, FAK and β -actin expression (Figure S6C). Total protein and protein phosphorylation levels were calculated in (C) and Figures S6D. SRC activation gene signature described by Bild *et al.* was scored using transcriptome of CD90^{low} and CD90^{high} GBM primary cell lines (D). CD90^{low} (yellow) and CD90^{high} (blue) GBM specimens from patients were tested for SRC phosphorylation by flow cytometry. Representative histograms and correlation between CD90 expression and SRC phosphorylation were presented in E and F respectively. (*): $p < 0.05$; (**): $p < 0.01$; (***) : $p < 0.001$.

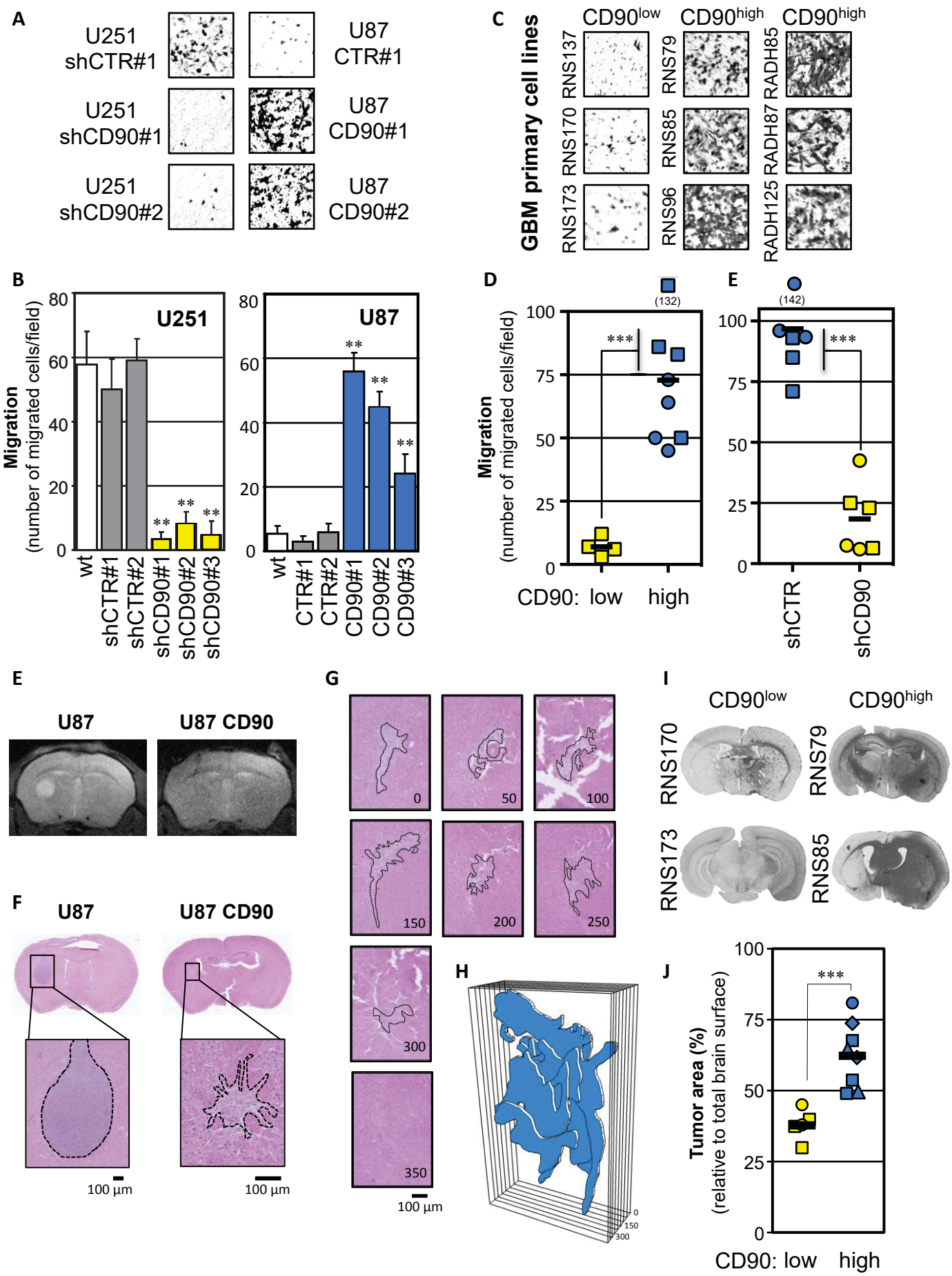
Figure 5: *CD90-dependent migration is altered by SRC, FAK, and ROCK kinases inhibitors.* CD90-expressing parental U251 and CD90#1 U87 cells were tested in a 24-hours Boyden chamber migration assay as described in Figure 2 in the presence of DMSO (as control, blank), PP2, dasatinib (both SRC inhibitors), Y15 (FAK inhibitor) and Y-27632 (ROCK inhibitor) (grey) (A). Migration was given by the number of migrated cells obtained per field. CD90^{high} RNS (n=4, square) and RADH (n=4, circle) cells were tested in a 24-hours Boyden chamber migration assay in the presence of DMSO (blue) or dasatinib (grey) (B and C). Representative fields are shown in (B). CD90 expressing U87 cells were orthotopically implanted in immunocompromised mice brain. One week after injection, mice were fed with control vehicle (n=7) or dasatinib (40 mg/kg/day, n=7) for 28 days. Control (n=4) and dasatinib-treated mice (n=4) were analyzed using MRI (D) and sacrificed 28 days after injection. Brains were collected and serial sections were analyzed after H&E staining (E and F). The tumor shape was reconstituted using SketchUp (G). (ns): non statistically different; (*): $p < 0.05$; (**): $p < 0.01$; (***) : $p < 0.001$.

Figure 6: *Dasatinib affects CD90-dependent cell-matrix adhesion of GBM cells and viability of CD90^{high} RNS cells.* Parental (wt, blank), control (shCTR#, grey), CD90-down expressing (shCD90#, n=3, yellow) U251 cells ; as well as parental (wt, blank), control (CTR#, grey) and CD90 expressing (CD90#, n=3, blue) U87 cells were tested in a cell attachment to collagen assay in the presence of 1 μ M dasatinib (A). Cell attachment inhibition was given the following formula: 100 x dasatinib / untreated condition. Adherent CD90^{low} and CD90^{high} RNS cells were grown in the presence of DMSO or dasatinib. Neurospheres morphology was observed after 14 days of culture (B). Adherent neurospheres were quantified in (C). CD90^{low} (yellow) and

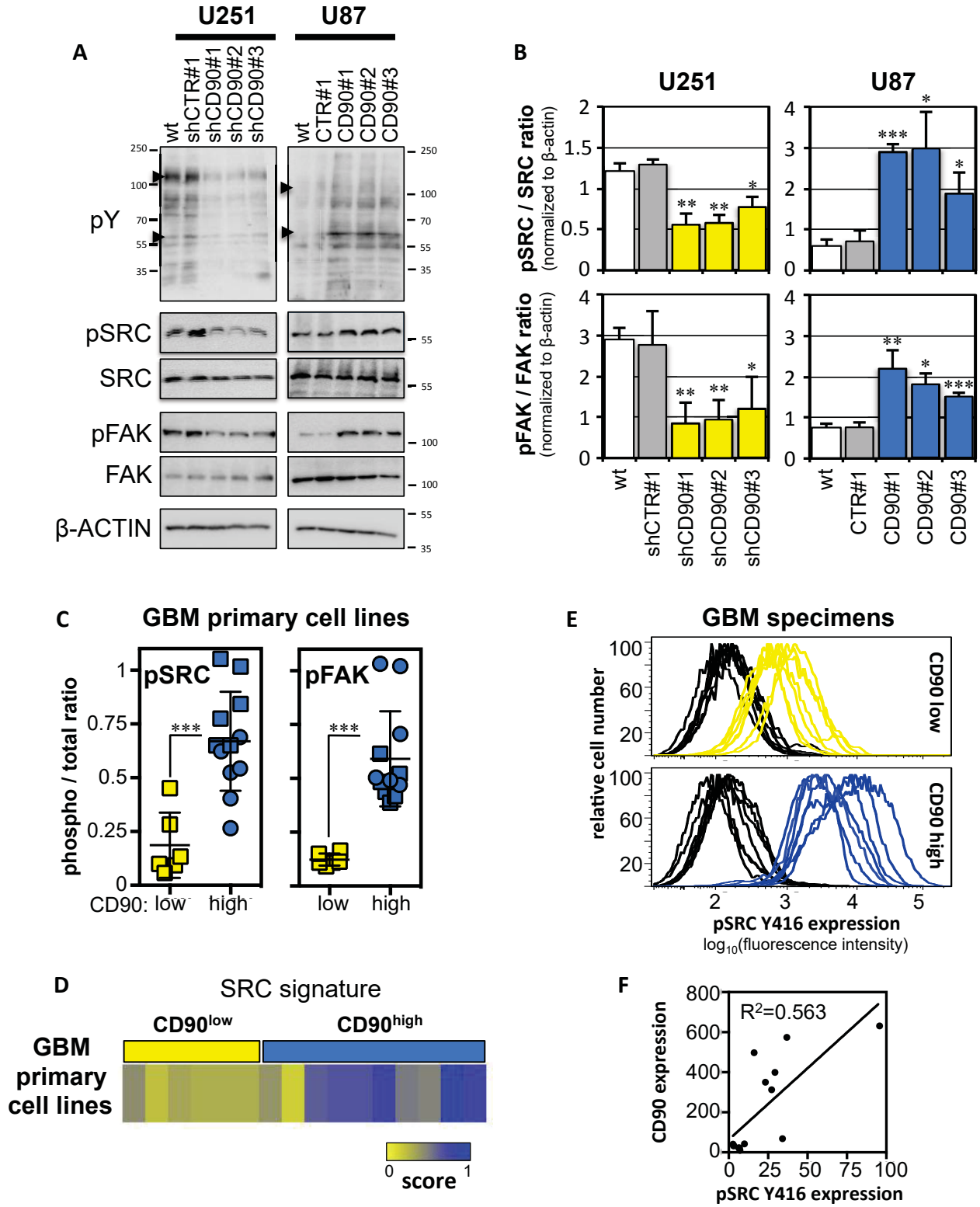
CD90^{high} (blue) RNS cells were cultured without or with dasatinib for 5 days and cell viability was determined (n=3; $p=0.009$ - ANOVA) (D). Corresponding CD90 expression levels and IC50 are indicated in (D). Control sh#CTR (blue) and CD90-down expressing sh#CD90 (yellow) RNS cells (n=3) cells were cultured without or with dasatinib and proliferation was determined as described in (D) ($p=0.003$ - ANOVA) (E). Schematic representation of dasatinib effects on GBM stem and non-stem cells described in this study was represented in (F). (*): $p < 0.05$; (**): $p < 0.01$; (***): $p < 0.001$.



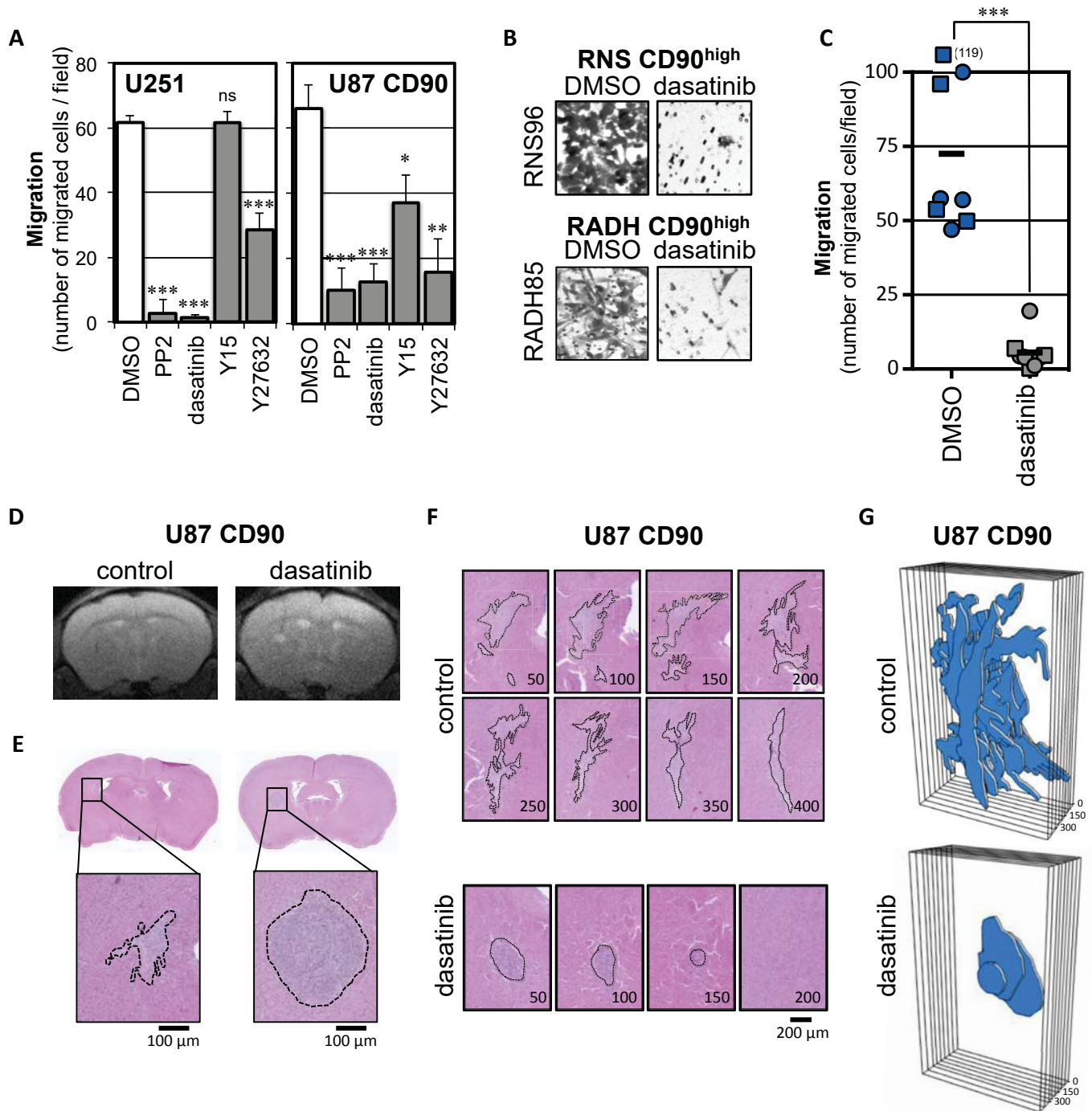


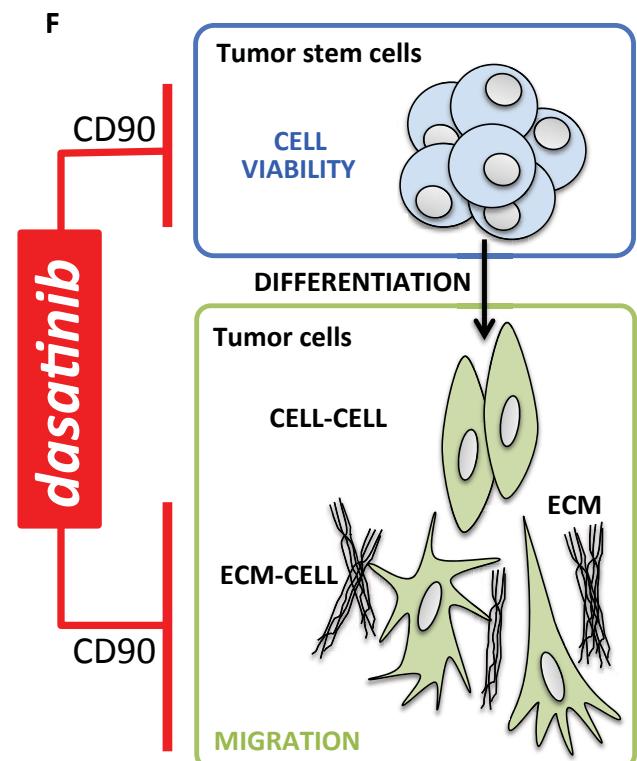
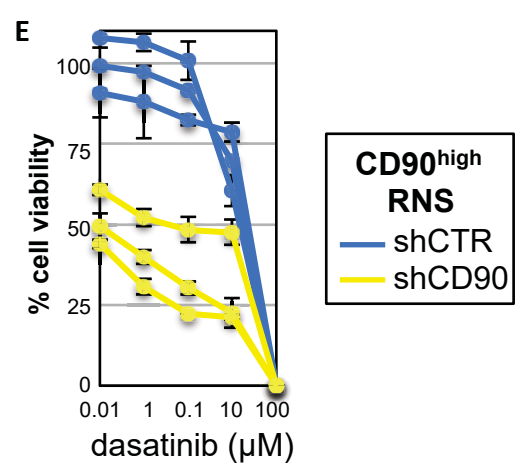
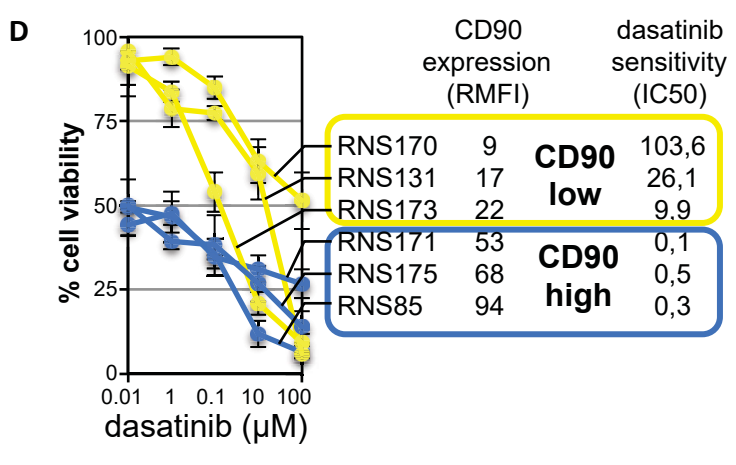
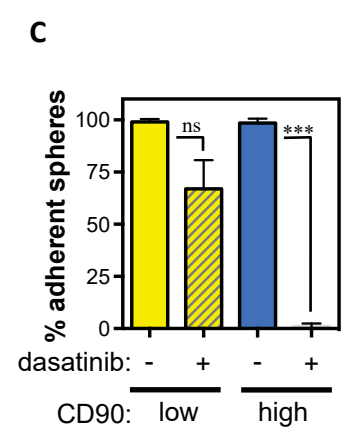
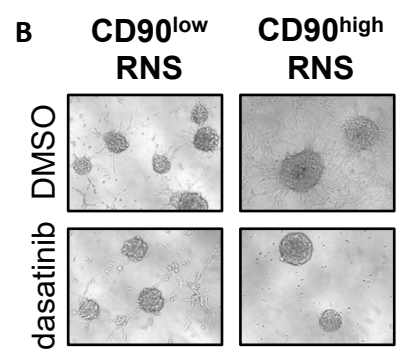
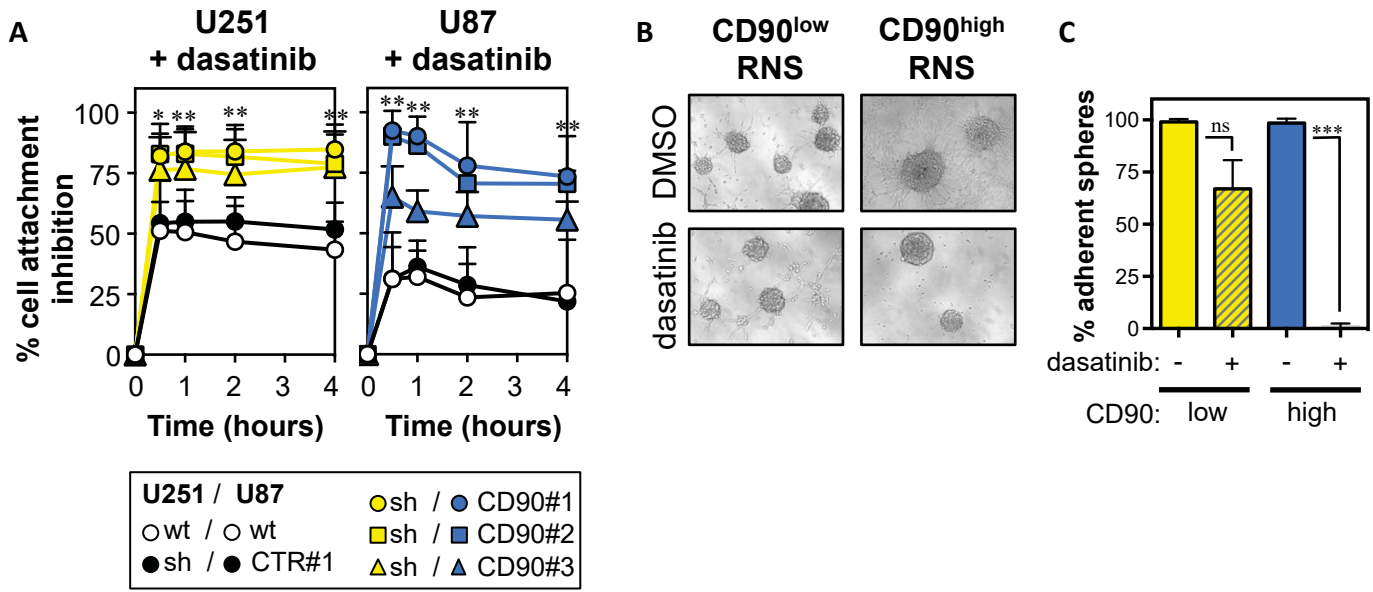


Avril et al. Fig 3



Avril et al. Fig 4





Avril et al. Fig 6

Clinical Cancer Research

CD90 expression controls migration and predicts dasatinib response in glioblastoma.

Tony AVRIL, Amandine Etcheverry, Raphaël Pineau, et al.

Clin Cancer Res Published OnlineFirst September 22, 2017.

Updated version	Access the most recent version of this article at: doi: 10.1158/1078-0432.CCR-17-1549
Supplementary Material	Access the most recent supplemental material at: http://clincancerres.aacrjournals.org/content/suppl/2017/09/22/1078-0432.CCR-17-1549.DC1
Author Manuscript	Author manuscripts have been peer reviewed and accepted for publication but have not yet been edited.

E-mail alerts	Sign up to receive free email-alerts related to this article or journal.
Reprints and Subscriptions	To order reprints of this article or to subscribe to the journal, contact the AACR Publications Department at pubs@aacr.org .
Permissions	To request permission to re-use all or part of this article, contact the AACR Publications Department at permissions@aacr.org .